Computational and Structural Biotechnology Journal 19 (2021) 3664–3672

COMPUTATIONAL AND STRUCTURAL BIOTECHNOLOGY JOURNAL

journal homepage: www.elsevier.com/locate/csbj

Method article

Computational modeling of microfluidic data provides high-throughput affinity estimates for monoclonal antibodies

Sonia Budroni [1], Francesca Buricchi [1], Andrea Cavallone [3], Gianfranco Volpini [5], Alessandra Mariani [4], Paola Lo Surdo, Christoph J. Blohmke, Giuseppe Del Giudice, Duccio Medini [2,*], Oretta Finco [2]

GSK, Siena, Italy

ARTICLE INFO

Article history:
Received 2 December 2020
Received in revised form 14 June 2021
Accepted 15 June 2021
Available online 17 June 2021

Keywords:
Microfluidic
Antibody affinity
Landau distribution
Gyrolab

ABSTRACT

Affinity measurement is a fundamental step in the discovery of monoclonal antibodies (mAbs) and of antigens suitable for vaccine development. Innovative affinity assays are needed due to the low throughput and/or limited dynamic range of available technologies.

We combined microfluidic technology with quantum-mechanical scattering theory, in order to develop a high-throughput, broad-range methodology to measure affinity. Fluorescence intensity profiles were generated for out-of-equilibrium solutions of labelled mAbs and their antigen-binding fragments migrating along micro-columns with immobilized cognate antigen. Affinity quantification was performed by computational data analysis based on the Landau probability distribution.

Experiments using a wide array of human or murine antibodies against bacterial or viral, protein or polysaccharide antigens, showed that all the antibody-antigen capture profiles (n = 841) generated at different concentrations were accurately described by the Landau distribution.

A scale parameter *W*, proportional to the full-width-at-half-maximum of the capture profile, was shown to be independent of the antibody concentration. The *W* parameter correlated significantly (Pearson's *r* [*p*–value]: 0.89 [3×10^{-8}]) with the equilibrium dissociation constant K_D, a gold-standard affinity measure.

Our method showed good intermediate precision (median coefficient of variation: 5%) and a dynamic range corresponding to K_D values spanning from ~10^{-7} to ~10^{-11} Molar. Relative to assays relying on antibody-antigen equilibrium in solution, even when they are microfluidic-based, the method's turnaround times were decreased from 2 days to 2 h.

The described computational modelling of antibody capture profiles represents a fast, reproducible, high-throughput methodology to accurately measure a broad range of antibody affinities in very low volumes of solution.

Author summary

High-affinity monoclonal antibodies are widely used for diagnostic, therapeutic and prophylactic purposes. Measuring the affinity of an antibody for its antigen is thus a critical parameter for the identification of new medicines and vaccines. Because currently available technologies have significant limitations in throughput, sample volume and dynamic range, there is a need for improved affinity assays. We used an existing immuno-assay technology in miniaturized compact-disk format as a basis to develop a computational model based on quantum physics theory, and used this model to quantify affinity. The method models the fluorescence intensity signal emanating from antibodies interacting with their immobilized target antigen. We validated this method using different concentrations of a large array of human or animal antibodies against bacterial or viral antigens of different biochemical nature. The affinity parameter derived from our experiments was found to correlate strongly with a well-characterized existing affinity parameter. The microfluidics-based approach was 20 times faster than the existing methodologies. In conclusion, the methodology

* Corresponding author.
E-mail address: duccio.medini@gmail.com (D. Medini).
[1] S.B. and F.B. contributed equally to this work.
[2] D.M. and O.F. have shared senior authorship.
[3] Current affiliation: Altran Italia, Expertise Center Big Data & Analytics, Turin, Italy.
[4] Current affiliation: Menarini Biotech, Pomezia (Rome), Italy.
[5] Current affiliation: Toscana Life Sciences Foundation, Via Fiorentina 1, 53100 Siena, Italy.

https://doi.org/10.1016/j.csbj.2021.06.024

offers great promise as a fast high-throughput tool, either to identify and screen new high-affinity antibodies for diagnostic or therapeutic use, or for use in the context of immunological studies.

1. Introduction

Affinity-matured, functional monoclonal antibodies (mAbs) are favored candidates for many successful prophylactic and therapeutic treatments, against various infectious diseases and conditions [1]. Having a high affinity for its target antigen is a prerequisite for a mAb to effectively exert its functionality against a given pathogen. Human antibody repertoires are an excellent source of functional mAbs, because they are naturally affinity-matured in response to an infection or vaccination, through an efficient B-cell selection process. However, highly potent mAbs are rare, and the field of mAb discovery for infectious diseases remains constrained by technical challenges of efficiently screening and capturing such mAbs. Affinity refers to the strength of a monovalent interaction between an epitope and a single complementarity-determining region on the binding site of the fragment antigen-binding molecule (Fab) [2,3] (this in contrast to avidity, *i.e.* the combined strength of multivalent interactions between the Fabs and one or more epitopes, which is the hallmark of most licensed vaccines [4]). The reversible bimolecular interaction defining affinity is determined by hydrophobic, electrostatic and/or van der Waals forces and hydrogen bonds. This interaction can therefore also be described in thermodynamic terms, as an equilibrium dissociation constant (K_D).

Immunoassays quantifying affinity can operate on the characterization of binding kinetics (association and dissociation rates), such as surface plasmon resonance (SPR) [5,6]. Alternatively, these assays rely on endpoint analysis, as is the case for enzyme-linked immunosorbent assay (ELISA) titration [7]. Drawbacks of the first category are the complicated measurement of the long dissociation times imposed by very high-affinity ($K_D \leq 10^{-12}$ M) binding, and the potential of artifacts due to mass-transport effects and steric hindrance of reagents [8]. ELISA-based methods can handle wider K_D ranges (10^{-13} to 10^{-07} M [9]), but are based on in-solution measurements performed after the equilibrium between antigen-bound and free antibodies has been reached [10]. These methods consequently require incubation times in the order of days, potentially leading to protein instability and buffer contamination [11,12]. Another obstacle is the requirement of high sample and reagent volumes. The latter challenge is addressed by the use of microfluidic technologies, such as the Gyrolab ligand-binding platform operating in an automated compact-disk (CD) format [13]. Affinity measurements based on this technology are derived from the distribution of fluorescence intensity (FI) changes ('capture profiles'). These profiles are detected when, due to centrifugal and capillary forces, fluorescent-labeled antibodies flow through and are captured onto antigen-coated microcolumns. However, the currently available equilibrium-based method still requires a pre-incubation step taking up to 48 h [14–16], rendering it unsuitable for rapid high-throughput measurements.

In the present study, we exploited the advantages of the microfluidic setting to develop a novel computational methodology to quantify affinity (here more broadly defined as the overall strength of the mAb/Fab—antigen interaction) *before* the system has reached equilibrium. Using a mathematical approach, affinity scores were computed based on an empirically detected similarity in curve shape between the capture profiles and a stable probability distribution, the Landau distribution [17]. This mathematical function belongs to the *General Extreme Value Distribution* class, and characterizes fluctuations of energy loss by ionization of charged particle beams passing through a thin layer of matter. Shortly after its introduction, an approximated version of the Landau distribution was developed. This version was subsequently shown to represent a "universal" descriptor of the energy-loss process in a number of different scattering regimes [18]. By fitting the approximated Landau distribution to the capture profiles generated for a large antibody-antigen panel, we explored the method's utility with respect to dynamic range, precision, and statistical correlation with the dissociation constant K_D, a gold-standard affinity measure. Our results suggest that this methodology is rapid, robust and high-throughput, and has broad applicability as an affinity-based screening tool of mAbs in human immunological studies.

2. Materials and methods

2.1. Antibody solutions

Gyrolab experiments were performed using solutions of purified mAb or Fabs (listed in Supplementary Table S1) at different concentrations, as specified in Supplementary data file 1. Solutions were made using Rexipp A or H buffer (Gyros cat #P0004820 or P0004822) for murine or human antibodies, respectively. No human or animal sera were used.

2.2. Binding assays using SPR

Binding affinities of the mAbs and Fabs against MenB antigens fHbp (10 mAbs, 7 Fabs), NHBA and NadA (3 mAbs each) were measured by SPR using a Biacore T200 instrument at 25 °C (GE Healthcare). For the single-cycle kinetics (SCK) experiments, commercially available Human Fab or Mouse Antibody Capture Kits (GE Healthcare) were used to covalently immobilize anti-human Fab antibodies or anti-mouse IgGs by amine coupling on a carboxymethylated dextran sensor chip (CM-5; GE Healthcare). Experimental running buffer contained 10 mM Hepes, 150 mM NaCl, 3 mM EDTA, 0.05% (vol/vol) P20 surfactant at pH 7.4. An average density level yielding ~8000–10,000 response units (RUs) was prepared for the immobilization on two flow cells of the CM5 chip. The immobilized IgGs were then used to capture between ~800–1200 RU of the tested mAbs or Fabs on the second flow cell. To determine the K_D and kinetic parameters, a titration series of five consecutive injections of increasing and variable analyte concentrations in the nanomolar range (spanning from 3.125 to 200 nM, flow rate: 40 μL/min) was performed, followed by a final surface regeneration step with 10 mM glycine pH 1.7–2 (180 s, flow rate: 10 μL/min). Antibody-coated surfaces without captured mAb were used as the reference channel. Signals using a blank injection (buffer only) were subtracted from each curve, and reference sensorgrams were subtracted from experimental sensorgrams to yield curves representing specific binding. The data shown in Fig. 3 are representative of at least two independent experiments. SPR data were analyzed using the standard SCK method [36] implemented by Biacore T200 evaluation software (GE Healthcare). Each sensorgram was fitted with the 1:1 Langmuir binding model, including a term to account for potential mass transfer, to obtain the individual k_{on} and k_{off} kinetic constants. Individual values were then combined to derive the single averaged K_D values reported. Additional details of SPR data analysis have been reported previously [37].

2.3. Gyrolab experiments

Experiments were performed on a Gyrolab workstation (Gyros). Biotinylated recombinant antigens were diluted in PBS with 0.01% Tween 20 and used as capture reagents at 100 μg/ml. Protein antigens were biotinylated using EZ-Link sulfo-NHS-LC-Biotin (Thermo Scientific, cat. #21335) at a molar excess of 10 mol biotsin: 1 mol

protein. Polysaccharidic antigens were biotinylated using EZ-Link Biotin-LC-Hydrazide (Thermo Scientific, cat. #21340) following manufacturer instructions. All antigens were internally produced. Using the standard Gyrolab capture-analyte-detect method [13], antibody solutions (as specified above) were run in dose–response curves to select the linear range (performed in triplicate), then used at a single concentration for affinity analysis (performed in 15 replicates).

The following Abs were used as detection reagent at 25 nM diluted in Rexipp F buffer (Gyros, cat. #P00004825): goat anti-human IgG, Fcγ fragment specific-Alexa 647 (Jackson cat. #109-605-098); goat anti-human IgG, Fab fragment specific-Alexa 647 (Jackson cat. #109-606-097); goat anti-mouse IgG, Fcγ fragment specific-Alexa 647 (cat. #Jackson 115-605-164). Wash station and pump solutions consisted of PBS with 0.01% Tween 20 (Sigma cat. #P1379). All mAbs were analyzed using Gyrolab Bioaffy 200 CDs (Gyros cat# P0004180) and standard Gyrolab three-step method [13]. The laser-induced fluorescence detector measures FI changes over the column. The *Gyrolab Viewer* software produces 3D visualization of the antibody-antigen capture profile in a heat-map format representing the FI as function of the transversal and radial direction of the flux. A 2D curve is then generated by integrating FI measurements along the transversal coordinate and reporting transversally integrated FIs against the 93 discreet radial coordinates of the CD, corresponding to the 93 laser scanning radii.

2.4. Modeling antibody-antigen capture profiles using an approximated Landau distribution

The 2D antibody-antigen capture profiles generated by the *Gyrolab Viewer* software were compared with the approximated Landau probability distribution $L(x)$ [18]:

$$L(x) = A \cdot \exp\left[-\frac{1}{2}\left(\frac{x - x_c}{W} + exp\left(-\frac{x - x_c}{W}\right)\right)\right] \quad (1)$$

where, according to the nomenclature of Fig. 1C, x is the radial coordinate along the column, x_c is the radial coordinate of the FI peak, W is a scale parameter proportional to the FWHM of the curve, and A is an overall normalization multiplier that, in the linear range of this assay as defined below, is proportional to the total FI.

To apply Eq. (1) to the current analysis method, we added a correction for experimental background noise (y_0), obtaining $L'(x)$:

$$L'(x) = y_0 + L(x) \quad (2)$$

as the mathematical representation of FI measured along the radial coordinate of the capture column. Non-linear regression was used to fit Eq. (2) to the data with the least-squares method as implemented in the *nls()* function in R version 3.3.1 [38]. All correlations, between experimental and fitted data as well as between W and K_D estimates, were evaluated using Pearson's correlation analysis, implemented in the *cor.test()* function in the same version of R.

2.5. Identification of the assay's linear response range

The linear response range of the assay comprised the range of values ξ of the antibody concentration in solution for which the overall FI generated was proportional to the concentration itself. To identify this range, each mAb or Fab solution was tested at multiple antibody concentrations (typically ≥ 7) to generate a dose–response curve, which was then compared with the four-parameter logistic (4PL) function:

$$f(\xi) = d + \frac{a - d}{1 + \left(\frac{\xi}{c}\right)^b} \quad (3)$$

where $f(\xi)$ is the response measured as total FI of the capture profile, ξ is the antibody concentration expressed in μg/mL, a is the minimum asymptote (*i.e.* the response at 0 μg/mL concentration), d is the maximum asymptote (*i.e.* the maximum response for a saturated solution), c is the logistic inflection point (*i.e.* the concentration for which the curve changes convexity, at the center of the linear range) and b is a slope factor (*i.e.* the steepness of the response curve in the linear range).

The least-square fit of the 4PL function to the W scores for the different concentrations was used to determine the values of the 4PL parameters. The concentration range to be considered effectively linear in the best fitting curve was determined according to the methodology described in [39], whereby the lower and upper concentrations ξ_{bend} delimiting as bending points the linear range are calculated as:

$$\xi_{bend} = c\left(\frac{a - y_{bend}}{y_{bend} - d}\right)^{-b} \quad (4)$$

where y_{bend} is either:

$$y_{bendlower} = \frac{a - d}{1 + \left(\frac{1}{k}\right)} + d, \text{ or : } y_{bendupper} = \frac{a - d}{1 + k} + d \quad (5)$$

and k = 4.6805 [39].

With simple algebra we obtain:

$$\xi_{bendlower} = c\left(\frac{1}{k}\right)^{-b}, \xi_{bendupper} = c\hat{A} \cdot k^{-b} \quad (6)$$

The region between the bend points $\xi_{bendlower}$ and $\xi_{bendupper}$is defined as the linear range of the assay.

2.6. Estimation of the W score

To determine the W score of an antibody-antigen pair, we selected only the 2D capture profiles generated for antibody concentrations falling in the linear response range. If <3 profiles would satisfy this condition, more profiles would be generated at the appropriate concentrations, in order to have at least 3 replicates. Eq. (2) was then fitted to the data of each capture profile independently, obtaining one estimate for the W score from each replicate. The affinity score of the antibody-antigen pair was then obtained as the arithmetic mean of the individual W values.

The above described methodology has been patented under WO2015014922 A3 [27]. Supporting data for all figures are presented in Supplementary Data File 1.

3. Results

3.1. FI profiles of microfluidic antibody-antigen interactions are analogous to an approximated Landau distribution

Our method for determining binding affinities derives from the 3D antibody-antigen interaction profiles generated by standard three-step (capturing molecule - analyte - detecting molecule [13]) Gyrolab methods. These profiles represent the FI values detected when antibodies in solution interact with their immobilized cognate antigen (Fig. 1A). From these profiles, 2D capture profiles were derived by reporting the integrated FI data measured along the longitudinal axis, versus the radial flux dimension along the 93 laser scanning points on the CD. Typically, a flat background FI signal from the first scanning points was followed by a sharp peak, and then a slower decrease with a long tail (Fig. 1B). After subtraction of the experimental background signal, the asymmetric curve shape was empirically considered as resembling the approximated Landau probability distribution (Fig. 1C). This function has as key determinants the x-coordinate at the FI peak (x_c),

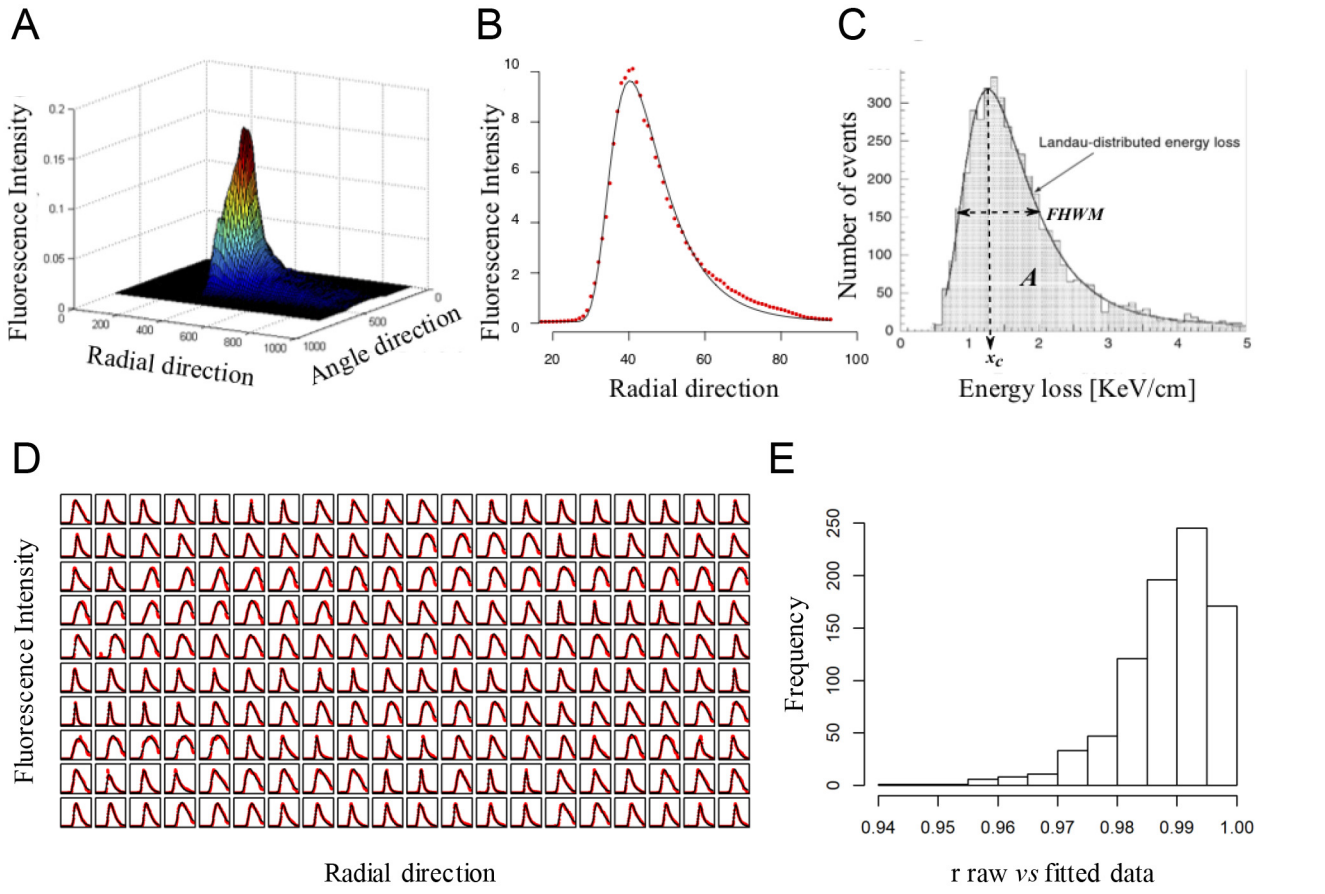

Fig. 1. The approximated Landau distribution accurately describes capture profiles from a broad panel of antibody-antigen pairs. (A) Example of a 3D visualization of the antibody-antigen capture profile in a heat-map format, as generated by Gyrolab Viewer software. Fluorescence intensity (FI) measurements on the vertical axis are shown *vs.* the radial direction (parallel to the flux) and the angle (transversal) direction. (B) 2D capture profile generated from the 3D data by integrating FI measurements over the transversal direction and plotting the integrated FIs against the radial coordinate of the CD (red dots). The approximated Landau distribution obtained as best fit of Eq. (2) to the data is shown as a black line. (C) Example of an approximated Landau distribution of the energy loss of electrons passing through a thin silicon layer [17]. A: area-under-the-curve. FWHM: full-width-at half-maximum. x_c: x-coordinate at peak. (D) Same as panel B, for a subset of 200 antibody-antigen pairs randomly selected from the main database of 841 profiles as detailed in Fig. S1 and Table S1. (E) Frequency distribution of Pearson's product-moment correlation coefficients (r) obtained by regression analysis between raw and fitted data for the 841 profiles shown in Fig. S1. (For interpretation of the references to color in this figure legend, the reader is referred to the web version of this article.)

and the parameters *W* and A. The latter two are proportional to the curve's full-width-at-half-maximum (FWHM) and the area under the curve, respectively. The application of this mathematical function to the experimental set-up is described by Eqs. (1) and (2) (Materials & Methods).

The observed resemblance led us to hypothesize that the Landau distribution provides a characterization that is generalizable to other antibody-antigen interactions tested in this setting. This hypothesis was tested by generating binding curves for a wide variety of antibody-antigen pairs. To this end, we used a panel of human or murine antibodies of different valencies combined with bacterial or viral, protein or polysaccharide coating antigens (83 mAbs/antigen, 53 Fabs/antigen; see Table S1). We then evaluated the impact of antibody concentration on the distribution. Testing each pair at multiple concentrations yielded 841 binding curves, after which the approximated Landau distribution was fitted to the raw data per pair, to determine the curves providing the best fit (Fig. S1; subset shown in Fig. 1D). Visual inspection of raw and best-fit curves consistently identified Landau-like-shaped curves across the array of antibody-antigen pairs and concentrations (with the best fit observed for profiles with a narrow peak). Moreover, when we evaluated the goodness-of-fit using regression analysis, the observed frequency distribution of Pearson's coefficients (Fig. 1E) indicated a strong correlation between raw and predicted data (r mean [95% CI]: 0.988 [0.967–0.998]). A slight decrease in the goodness of fit was observed for curves with higher *W*, with r mean going from 0.996 at W = 2 to 0.978 at W = 14, as shown in Fig. S2. However, all correlations had strong statistical significance (all *p-values* < 10^{-10}) and the very high correlation coefficients supported the generalizability of the model across the entire range of observed *W*.

Overall, the data confirmed that in this microfluidic experimental setting, the proposed mathematical function can be applied to faithfully characterize FI profiles of antibody-antigen interactions, irrespective of the biochemical nature of the antigen, or the valency of the antibody. Interestingly, the Landau-like curve shape, of which the *W* parameter is a key determinant, was detected irrespective of the concentration of antibodies in solution, leading to a deeper investigation of the relationship between *W* and concentration.

3.2. W scores are concentration-independent

To accurately determine whether concentration can affect the *W* score, we selected five antibody-antigen pairs representative of the dataset's diversity (Table S1). We generated capture profiles at seven different antibody concentrations per pair (except for one pair which was tested at 14 concentrations). For each pair, we used

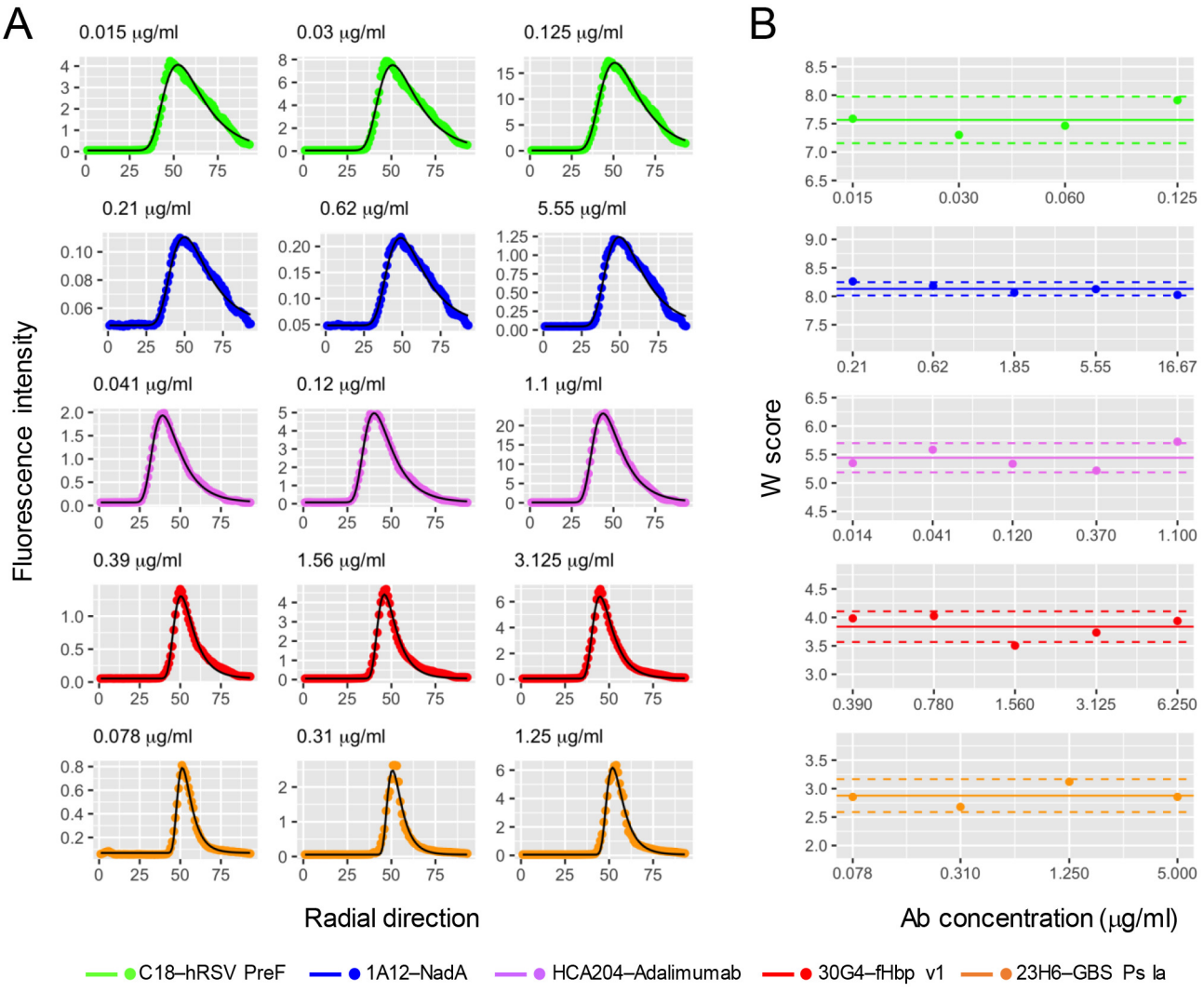

Fig. 2. The *W* score is independent from the antibody concentration. Each row shows data for a different antibody-antigen pair. Green: mAb C18 - human respiratory syncytial virus prefusion F protein (hRSV PreF). Blue: Fab 1A12 – *N. meningitidis* serogroup B (MenB) adhesin A (NadA). Purple: mAb HCA204 - human mAb Adalimumab. Red: mAb 30G4 - MenB fHbp protein. Orange: mAb 23H6 - Group B Streptococcus capsular polysaccharide serotype Ia (GBS Ps Ia). Each pair was tested at 14 (mAb 30G4) or 7 (other Abs) concentrations. (A) Graphs show, for the antibody concentration indicated, 2D capture profiles (colored dots) and the approximated Landau distribution obtained as best fit of Eq. (2) to the data (black lines). Three concentrations within the linear range were randomly selected for each antibody-antigen pair. (B) *W* scores obtained for each antibody concentration within the linear range are shown as colored dots *vs.* the concentration itself. Arithmetic means of *W* scores (solid lines) with 95% confidence intervals (dashed lines) are indicated. (For interpretation of the references to color in this figure legend, the reader is referred to the web version of this article.)

Eqs. (3) and (4) (see Materials and Methods) to determine the linear binding range, *i.e.* the range where the antibody concentration is proportional to the total FI level of the capture profile. Per pair, we then generating profiles for at least four different concentrations (ranging across pairs from 0.014 to 17 μg antibody/mL) within the respective linear binding range.

Fig. 2A shows, for each antibody-antigen pair, three of the generated binding profiles for a given antibody concentration within the linear range. Landau-like curves were observed for all pairs and concentrations. While, as expected, FI peaks increased with the concentration, curve widths remained constant across the concentration range. Accordingly, the *W* scores remained independent from concentration, as shown by plots of *W* scores *vs.* antibody concentrations generated per pair (Fig. 2B). The absence of a concentration effect on *W* was statistically supported by linear regression between antibody concentrations and *W* scores, yielding slope coefficients that were all not significantly different from zero.

Overall, the data indicated that the *W* score represents a concentration-independent, intrinsic characteristic of the antibody-antigen binding, suggesting that the parameter may be related to the affinity of this binding.

3.3. W Score is a robust and high throughput estimator of affinity

To further explore the correlation between Landau peak width at half height and antigen binding, we considered the FI profiles and corresponding Landau curves produced for three different antibodies with either a high, moderate or a low affinity for the same *Neisseria* adhesin A (NadA) antigen (K_D values: 10^{-10}, 10^{-09} or 10^{-08} M, respectively) as shown in Fig. 3A. Higher binding affinity appeared to be associated with sharper curves, *i.e.* smaller FWHM values and *W* scores. This observation could be explained by a faster binding along the radial coordinate.

To validate the inverse relationship between *W* and antibody affinity for the antigen, we generated *W* scores and K_D values, at one or more repeats each, for a panel of 23 antibodies against either *Neisseria* Heparin-Binding Antigen (NHBA, 3 mAbs), NadA (3 mAbs), or factor H binding protein (fHbp; 10 mAbs, 7 Fabs);

see Fig. 3B. The highest affinities measured ($K_D \approx 10^{-11}$ M) corresponded to a *W* score of approximately 4, while the lowest affinities ($K_D = 10^{-8}$ to 10^{-7} M) corresponded to *W* scores between approximately 11 and 12. A least-squares regression comparing ($\log_{10}$-tranformed) *W* scores and K_D values across the entire range, demonstrated a highly significant, linear correlation (Pearson's *r* [*p*-value]: 0.78 [1.12×10^{-5}]). Only one of the 23 antibodies tested (an anti-fHbp mAb; circled in Fig. 3B) generated both a low K_D value (4.6×10^{-9} M) and a low *W* score (4.2), with a mean that was five standard deviations higher than the confidence range of the regression. Because only a single experimental K_D value could be generated for this mAb, we considered the result as a potential outlier eligible for removal. Reanalysis of the correlation yielded a Pearson's *r* of 0.89 (*p*-value = 3.56×10^{-8}). Overall, the data were indicative of a broad dynamic range spanning *W* scores from ~ 4 to 12 corresponding to K_D values from 10^{-8} to 10^{-11} M, with high-affinity ($K_D < 10^{-10}$ M) antibodies corresponding to *W* scores < 5.

We then evaluated assay precision. Assessments were performed on *W* scores obtained by repeated testing of the same antibody-antigen pair, either within the same CD (within-assay/CD variability, *i.e.* repeatability) or between different CDs (between-assay/CD variability, *i.e.* intermediate precision). Fig. 4A shows the repeatability of *W* scores (range: 2.8—12.4) derived from 3 to 16 technical repeats performed for each antibody-antigen pair from a subset (n = 76) of the larger panel (see Supplementary Data File 1). The coefficients of variation (CVs) followed the typical U-shaped curve of immunoassays, showing lower variability at intermediate values of the measured parameter, and higher variability at the extremes of the parameter's range. Overall, repeatability was reasonably low (median/maximum CV: 5%/18%). Between-assay variability (Fig. 4B) was assessed by testing 10 Ag/Ab pairs from the same subset, in three or four independent runs (different CDs). Per run, each pair was tested in ≥ 3 technical replicates per CD. Within-run estimates of *W* were averaged to determine the overall *W* score of the given run, and within-CD averages were compared by least-squares regression to determine between-run CVs. As compared with the within-assay measurements, the range of variability was reduced, with no obvious trend toward extreme *W* scores (median/maximum CV: 5%/11%). The data were indicative of a good assay intermediate precision, and supported the feasibility of an experimental protocol based on a single CD, with multiple technical repeats to be averaged within the same CD. Overall, assay precision appeared to be independent from the *W* score, which was shown to be a homoscedastic and highly reproducible parameter. Given the overall ~10% assay precision and the experimental range, *W* estimates are reported with one significant figure.

Finally, by applying the described experimental protocol, we achieved accurate affinity measurements for 14 mAbs (the maximum number of pairs processable per CD [19]) within 2 h by two runs of a single CD, using less than 5 μL per sample. This highlighted the quick turnaround time and low sample volume requirement of our approach. Collectively, the data indicated that the presented *W* score-based affinity measurements, derived by fitting an approximated Landau distribution on microfluids-based FI capture profiles, is a robust, high-throughput, and fast methodology, applicable to a wide range of affinities of mAbs or Fabs in low sample volumes.

4. Discussion

Recent years have seen a rise in innovative technologies for B-cell isolation, interrogation of the human repertoire, and generation of recombinant antibodies. This created a surge in numbers of mAbs to be tested and characterized for one of their key features, the affinity of binding to the target antigen. Affinity measurement is thus a critical step in the evaluation of mAbs for diagnostic or prophylactic applications, and may also be key to select mAbs for use in the identification of microbial antigens suitable for vaccine development. Considering the caveats of currently available technologies to quantify affinity [8,12,14,15,20], there is a need for a rapid high-throughput method using low quantities of antibody, to allow efficient characterization of large numbers of mAbs. We developed a computational approach based on data generated by a microfluidic system. In our approach, FI profiles characterizing the antibodies' capture onto antigen-coated microcolumns, are fitted to an asymmetric probability function (the approximated Landau distribution), from which an affinity score *W* is computed. We then assessed assay performance across a range of antibody-antigen combinations and antibody concentrations.

The Landau-like profile was chosen empirically, due to its morphological analogy with the experimental fluorescence intensity profiles. Other skewed distributions potentially achieving similar or better goodness of fit were not explored, as the model was widely applicable across a highly diverse array of antibody-antigen pairs. It was consistently observed irrespective of the species (bacterial or viral) and chemical nature (proteic or polysaccharidic) of the antigen, and the valency (mAbs or Fabs) of the antibody. Although possibly coincidental, the breadth of this spectrum suggests that the underlying dynamics of capture along the microfluidic column may share some fundamental analogy with the quantum–mechanical process of energy loss for charged particles through matter, for which the Landau distribution was originally developed [17].

Deriving the Landau approximated function from the generative process of the current microfluidic setup could help clarifying the analogy, but the modeling effort exceeds the scope of the present work. Significant differences between the quantum–mechanical and the microfluidic system do exist. In the quantum–mechanical process of ionizing particles traversing matter, the variable exhibiting a Landau distribution is the energy lost by the incoming particles (see Fig. 1C), which is assumed small versus the incoming particles energy. In our microfluidic process, the Landau-distributed variable is the horizontal coordinate at which the antibody is captured by the coated antigen. Indeed, the horizontal coordinate along the capture column may be considered a proxy for the kinetic energy lost by the antibodies flowing through the column. Intuitively, the faster the antibody is injected into the column, the farther it will travel before its capture. Since at the end of the process every captured antibody is immobilized on the column, those that were captured last will be the ones that have lost the highest amount of kinetic energy, and *vice versa*.

In the quantum–mechanical process, the equivalent of our *W* (*Q* in the notation of [18]) is the mean number of collisions, *i.e. the primary ionization*, and is approximately proportional to the length of the material traversed. The thicker the material the broader the curve, since the increasing number of interactions augments the likelihood of particles loosing higher amounts of energy, hence broadening the tail of the distribution.

The *W* score derived from our methodology was, like the affinity gold standard measure K_D, a concentration-independent parameter, representing an intrinsic quality of the given antibody-antigen pair: the weaker the interaction, the broader the curve. In the microfluidic column the kinetic energy of the antibodies flowing through the antigen lattice is reduced by random hits, until the chemical potential of the epitope-epitome interaction (affinity) exceeds the residual kinetic energy, and the antibody is captured. A stronger affinity will achieve the capture sooner, *i.e.,* after a smaller number of interactions, as if the microcolumn was *effectively*

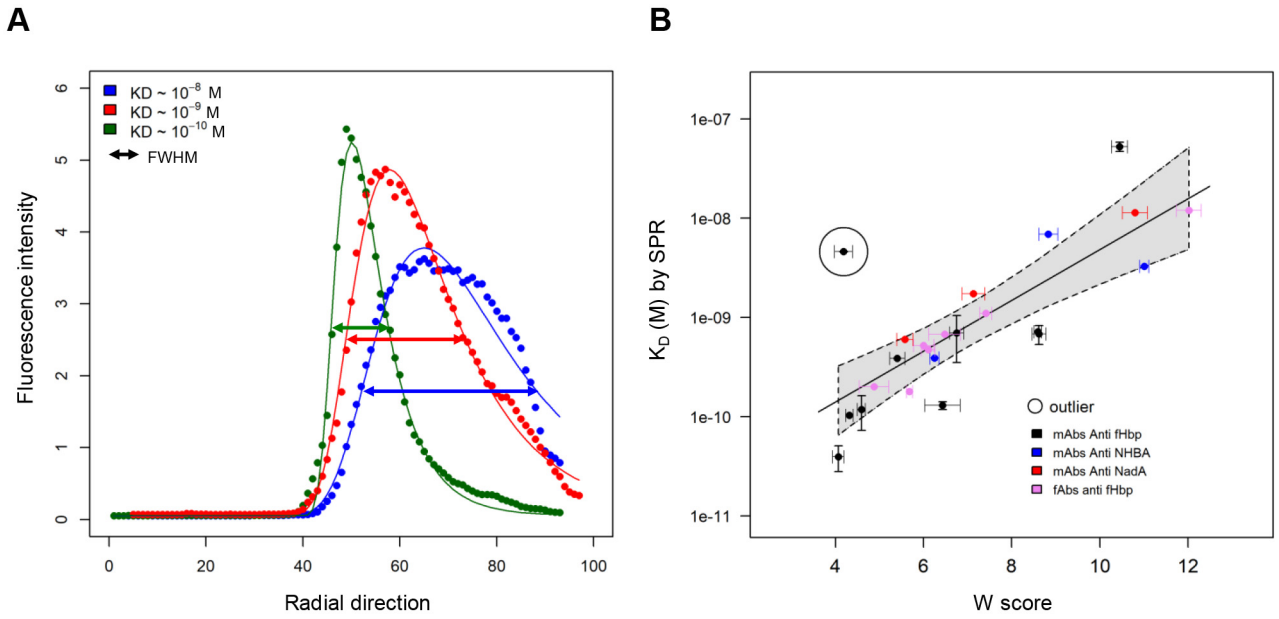

Fig. 3. Relationship between the affinity constant K_D and the *W* score. (A) Plots represent 2D capture profiles (represented by colored dots) generated for three antibodies against the *N. meningitidis* NadA protein with either a high (green, $K_D \sim 10^{-10}$ M), medium (red, $K_D \sim 10^{-09}$ M) and low (blue, $K_D \sim 10^{-08}$ M) affinity. Corresponding approximated Landau best fit curves are represented by solid lines of the same color. FWHM: full-width-at half-maximum. (B) *W* scores (x-axis) and K_D values (y-axis) for antibodies against *N. meningitidis* antigens are presented, comprising 10 mAbs against fHbp (black), 3 mAbs against NHBA (blue), 3 mAbs against NadA (red) and 7 Fabs against fHbp (pink). Color-coded symbols and horizontal or vertical bars represent means and standard errors of the associated *W* and K_D values. Solid straight line: least-square linear regression of K_D *vs. W*. Grey-shaded area: 95% confidence interval of the linear regression. (For interpretation of the references to color in this figure legend, the reader is referred to the web version of this article.)

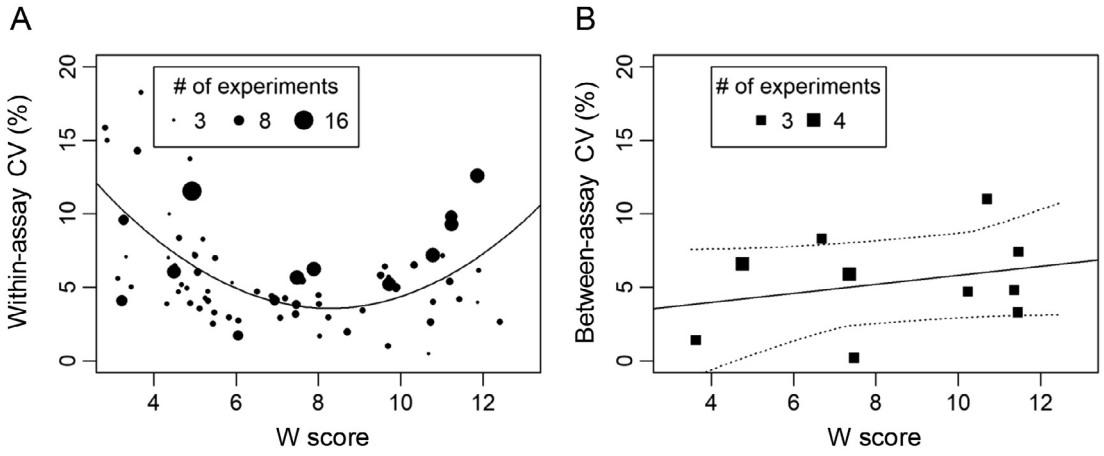

Fig. 4. Assay precision. (A) Repeatability: within-assay coefficients of variation (CVs) are plotted against the *W* scores derived from 76 mAbs/Fabs tested at least three times within the same experiment. Symbol sizes are proportional to the number of replicates (3–16) per experiment. The curve is a quadratic fit to the data. (B) Intermediate precision: between-assay CVs are plotted against *W* scores derived for 10 mAbs/Fabs, each tested in three or four independent experiments. Least-squares linear regression with 95% confidence intervals are shown as solid and dotted lines, respectively.

shorter, while a weaker affinity will allow for more hits, as for an *effectively* thicker column, confirming the analogy with the quantum–mechanical system.

These observations may expand the "universal" character of the Landau distribution originally observed for charged particles [18] into the domain of biological macromolecules, suggesting the presence of a scaling property applicable across physics and biochemistry that warrants further investigation.

The dynamic range of *W* explored in the present work was comparable to that found for existing methods; assay precision (median intermediate precision: 5%) and accuracy were satisfactory, given the robust correlation between the *W* score and K_D (Pearson's *r* [*p*-value]: 0.89 [3×10^{-8}]), that was measured in an SPR affinity set-up (see Materials and Methods). Although the experimental set up of the microfluidic platform was also geared towards measuring monovalent Ag-Ab interactions, *i.e.* affinity, we cannot exclude the possible contribution of cooperativity effects induced by bi-valent bonds between the two Ab fragments and the antigenic substrate, that would introduce an avidity component in the readout. The good correlation with SPR-derived affinity measurements, the out-of-equilibrium characteristic of the method, the high concentration of antibodies in the solution flowing through the micro-column that creates a strong competition for the substrate and the spacing among the microbeads that favours monovalent interactions, all suggest that *W* should be considered a proxy for affinity rather than avidity. In an attempt to further clarify this point, within the limited dataset available, we compared *Ws* obtained for matched Fabs and mAbs against the same

antigens (see the Supplementary Table S2). With four monomeric antigen proteins we observed a substantially identical *W* against eleven Fab/mAb pairs (all ratios W(Fab)/W(mAb) between 0,9 and 1,2, well within the experimental variability of the assay, except one ratio = 1,4) confirming that mAbs establish along the column mainly monovalent links with their substrate, determining an affinity measurement. Against an omo-trimeric antigen protein tested against 4 matched Fabs/mAbs the ratio W(Fab)/W(mAb) ranged from 1,3 to 2,5 suggesting that bi-valent interactions could become more relevant for multimeric substrates. However, the diverse, non-standardized expression and purification systems used for Fabs and mAbs in the present study may significantly affect the measurement, suggesting that an ad-hoc study would be required for a conclusive assessment.

Recently, the manufacturer of the platform released a commercial software called Gyrolab™ Affinity Software Module, to estimate affinity from in-solution equilibrium-based methods. The main advantages of the microfluidic affinity assay in its standard equilibrium-based format are the minimal sample/reagent volumes, and the limited operator involvement and laboratory work due to the automated system [13]. Its main limitation lies in the turnaround time, given that the required preincubation step can take up to two days [14–16]. Our approach retains all the above-mentioned advantages while circumventing this time-consuming preparatory step. This allows linking the increased productivity to a high throughput, as demonstrated by the 2-hour total turnaround time needed to process 14 mAbs in duplicate runs. In addition, the obtained assay precision may even invite exploring the feasibility of reducing the number of repeats in certain cases (as proposed for Gyrolab-based IgG measurement in a regulatory context [21]) as a means to further accelerate the analyses. Moreover, in our out-of-equilibrium setting the accidental presence of multiple monoclonals with different affinities in the same sample is detected as a deviation from the Landau-curve fit, while in solution equilibrium-based settings the monoclonal with higher affinity is likely to dominate the binding signal and the contamination to go un-noticed. Finally, we observed that the adherence of the capture profiles to the Landau distribution increased at higher affinities. As a consequence, the dynamic range (corresponding to K_D values of 10^{-7} to 10^{-11} M, comparable to equilibrium-based microfluidic affinity testing [19]) may be extended to include *W* scores equivalent to K_D values of 10^{-12} M or beyond. Collectively, this suggests that our approach offers a valuable tool to perform a first, rapid high-throughput screening for high affinity binders. Lead molecules can then be further characterized, including precise affinity determination, with standard methods such as SPR or Bio-Layer Interferometry (BLI), significantly accelerating the identification of the best mAbs. The short turnaround time also caters to the demands of emergency situations requiring rapid high-throughput affinity screening of multiple mAbs, for example to support the immunological data-sets required to fast-track clinical trial approvals for biotherapeutics. This may be relevant for screening of mAbs in the context of pandemics of infectious diseases, e.g. those against SARS-CoV-2 for therapeutic or prophylactic uses, or mAbs against cytokines involved in COVID-19 pathology for use as post-exposure treatment [22,23]. Additionally, the assay can be utilized in the context of antimicrobial resistance, to screen mAbs for use as highly pathogen-specific alternatives to antibiotics, such as those described in [24,25]. In the vaccine context, the method has already been successfully applied to dissect the human antibody response to a multicomponent MenB vaccine, by profiling the affinity of binding to different target antigens of Fabs isolated from single B cells from vaccinees [26]. Lastly, we note that the current work presents, to the best of our knowledge, the first description of computational modeling of antibody affinity based on a Landau distribution.

5. Conclusion

By basing our computational model to quantify antibody affinity on an existing microfluidic technology, we capture a wide range of affinities in a rapid, precise and high-throughput manner, while consuming minimal amounts of reagents. This method has broad-range applicability as an effective tool for affinity-based screening of mAbs and their fragments to identify and characterize novel biotherapeutics, and for use in the context of human immunological studies.

An enticing future perspective is to extend the use of the mAbs/Fab-based method to the measurement of avidity of polyclonal antibody responses in serum from immunized or naturally infected subjects. This could be achieved by applying a deconvolution algorithm to capture profiles from polyclonal samples, allowing identification of profiles of subpopulations of mAb-like clones, which can then be characterized for their avidity and abundance [27]. Avidity reflects the level of B-cell maturation upon antigenic stimulation, driving antibody functionality [28,29]. Hence, *W* score-based information can be used to monitor avidity maturation in clinical vaccine development, e.g. to complement Gyrolab-based anti-SARS-CoV-2 antibody levels elicited by COVID-19 vaccines [30]. The method's practical value is exemplified by recent analysis of clinical trial samples from recipients of adjuvanted vaccines (submitted manuscript) in the context of studies comparing immune responses between different licensed adjuvants [31–33]. Finally, given the robust correlation with the K_D observed for mAb/Fab-based analyses, the adapted methodology may also offer a major advantage over the commonly used chaotrope-based avidity indices, for which such correlation is not consistently observed [34,35].

CRediT authorship contribution statement

Sonia Budroni: Conceptualization, Data curation, Formal analysis, Investigation, Methodology, Software, Validation, Visualization, Writing - original draft, Writing - review & editing. **Francesca Buricchi:** Conceptualization, Data curation, Investigation, Writing - original draft, Writing - review & editing. **Andrea Cavallone:** Investigation. **Gianfranco Volpini:** Investigation. **Alessandra Mariani:** Investigation. **Paola Lo Surdo:** Investigation. **Christoph J. Blohmke:** Writing - review & editing. **Giuseppe Del Giudice:** Investigation, Supervision, Writing - review & editing. **Duccio Medini:** Conceptualization, Project administration, Supervision, Writing - original draft, Writing - review & editing. **Oretta Finco:** Conceptualization, Project administration, Supervision, Writing - original draft, Writing - review & editing.

Declaration of Competing Interest

SB, FB, GV, PLS, CJB, GDG, DM and OF are (or were at the time of writing) employees of the GSK group of companies. AC and AM participated in a post graduate studentship program at GSK at the time of the study. GDG, DM and OF report ownership of GSK shares and/or restricted GSK shares as part of his/her employee remuneration at the time of writing.

Acknowledgement

The authors thank Jacopo Franco for helping exploring the analogy between immunologica and quantum-mechanical processes; Ellen Oe and Inge van Dyck (both GSK) for providing scientific writing services in the manuscript's development, and publication management, respectively.

Financial disclosure statement

This work was sponsored by GlaxoSmithKline Biologicals SA which was involved in all stages of the study conduct and analysis.

Appendix A. Supplementary data

Supplementary data to this article can be found online at https://doi.org/10.1016/j.csbj.2021.06.024.

References

[1] Castelli MS, McGonigle P, Hornby PJ. The pharmacology and therapeutic applications of monoclonal antibodies. Pharmacol Res Perspect 2019;7(6).
[2] Chung AW, Alter G. Systems serology: profiling vaccine induced humoral immunity against HIV. Retrovirology 2017;14:57.
[3] Chan TD, Brink R. Affinity-based selection and the germinal center response. Immunol Rev. 2012; 247: 11–23.
[4] Wang XY, Wang B, Wen YM. From therapeutic antibodies to immune complex vaccines. npj Vaccines 2019;4:2.
[5] Murphy M, Jason-Moller L, Bruno J. Using Biacore to measure the binding kinetics of an antibody-antigen interaction. Curr Protoc Protein Sci 2006;45(1). Unit 14.
[6] Leonard P, Hearty S, O'Kennedy R. Measuring protein-protein interactions using Biacore. Methods Mol Biol 2011;681:403–18.
[7] Bobrovnik SA. Determination of antibody affinity by ELISA. Theory J Biochem Biophys Methods 2003;57(3):213–36.
[8] Kortt AA, Gruen LC, Oddie GW. Influence of mass transfer and surface ligand heterogeneity on quantitative BIAcore binding data. Analysis of the interaction of NC10 Fab with an anti-idiotype Fab'. J Mol Recognit 1997;10:148–58.
[9] Bee C, Abdiche YN, Stone DM, Collier S, Lindquist KC, Pinkerton AC, et al. Exploring the dynamic range of the kinetic exclusion assay in characterizing antigen-antibody interactions. PLoS One. 2012; 7: e36261.
[10] Blake RC, Pavlov AR, Blake DA. Automated kinetic exclusion assays to quantify protein binding interactions in homogeneous solution. Anal Biochem 1999;272(2):123–34.
[11] Drake AW, Myszka DG, Klakamp SL. Characterizing high-affinity antigen/antibody complexes by kinetic- and equilibrium-based methods. Anal Biochem 2004;328(1):35–43.
[12] Darling RJ, Brault P-A. Kinetic exclusion assay technology: characterization of molecular interactions. Assay Drug Dev Technol 2004;2(6):647–57.
[13] Mora JR, Obenauer-Kutner L, Vimal Patel V. Application of the Gyrolab™ platform to ligand-binding assays: a user's perspective. Bioanalysis 2010;2(10):1711–5.
[14] Salimi-Moosavi H, Rathanaswami P, Rajendran S, Toupikov M, Hill J. Rapid affinity measurement of protein-protein interactions in a microfluidic platform. Anal Biochem 2012;426(2):134–41.
[15] Eriksson C, Agaton C, Kånge R, Sundberg M, Nilsson P, Ek Bo, et al. Microfluidic analysis of antibody specificity in a compact disk format. J Proteome Res 2006;5(7):1568–74.
[16] Dai Z, Juneja J, Schneeweis L, Cohen D, Marsilio F, Morin P, et al. Application of the Gyrolab microfluidic platform to measure picomolar affinity of a PD-L1-binding Adnectin radioligand for positron emission tomography. Biotechniques 2020.
[17] Landau L. On the energy loss of fast particles by ionization. J Phys (USSR) 1944;8:201–5.
[18] Moyal JE. Theory of ionization fluctuations. London, Edinburgh, Dublin Philos Magazine J Sci 1955;46:263–80.
[19] Gyros Protein Technologies. In-solution affinity determination using Gyrolab systems. Technical Note no. D0025522/B; 2020.
[20] Estep P, Reid F, Nauman C, Liu Y, Sun T, Sun J, et al. High throughput solution-based measurement of antibody-antigen affinity and epitope binning. MAbs 2013;5(2):270–8.
[21] Barfield M, Goodman J, Hood J, Timmerman P. European Bioanalysis Forum recommendation on singlicate analysis for ligand binding assays: time for a new mindset. Bioanalysis 2020;12(5):273–84.
[22] Marovich M, Mascola JR, Cohen MS. Monoclonal antibodies for prevention and treatment of COVID-19. JAMA 2020;324(2):131. https://doi.org/10.1001/jama.2020.10245.
[23] Pinto D, Park Y-J, Beltramello M, Walls AC, Tortorici MA, Bianchi S, et al. Cross-neutralization of SARS-CoV-2 by a human monoclonal SARS-CoV antibody. Nature 2020;583(7815):290–5.
[24] Saylor C, Dadachova E, Casadevall A. Monoclonal antibody-based therapies for microbial diseases. Vaccine 2009;27(Suppl 6):G38–46.
[25] Ghosh C, Sarkar P, Issa R, Haldar J. Alternatives to conventional antibiotics in the era of antimicrobial resistance. Trends Microbiol 2019;27(4):323–38.
[26] Giuliani M, Bartolini E, Galli B, Santini L, Lo Surdo P, Buricchi F, et al. Human protective response induced by meningococcus B vaccine is mediated by the synergy of multiple bactericidal epitopes. Sci Rep 2018;8(1). 3700.
[27] Finco O, Budroni S, Buricchi F, Medini D, Volpini G. Method for measuring binding reactions. International patent no. WO2015/014922A2. 2015; PCT/EP2014/066445.
[28] Plotkin SA, Orenstein WA, Offit PA. Vaccines. 5th ed. Philadelphia, PA: Elsevier Inc; 2008.
[29] Bottermann M, Lode HE, Watkinson RE, Foss S, Sandlie I, Andersen JT, et al. Antibody-antigen kinetics constrain intracellular humoral immunity. Sci Rep 2016;6(1). 37457.
[30] Gyros Protein Technologies. Available at: Immunoassays for COVID-19 Research and Vaccines; 2020.
[31] Leroux-Roels G, Marchant A, Levy J, Van Damme P, Schwarz TF, Horsmans Y, et al. Impact of adjuvants on $CD4^+$ T cell and B cell responses to a protein antigen vaccine: results from a phase II, randomized, multicenter trial. Clin Immunol 2016;169:16–27.
[32] Burny W, Callegaro A, Bechtold V, Clement F, Delhaye S, Fissette L, et al. Different adjuvants induce common innate pathways that are associated with enhanced adaptive responses against a model antigen in humans. Front Immunol 2017;8. 943.
[33] De Mot L, et al. Transcriptional profiling of adjuvanted vaccines: variable interindividual homogeneity, but core signature linked to antibody responses. Sci Transl Med. 2020; In press.
[34] Alexander MR, Ringe R, Sanders RW, Voss JE, Moore JP, Klasse PJ, et al. What do chaotrope-based avidity assays for antibodies to HIV-1 envelope glycoproteins measure?. J Virol 2015;89(11):5981–95.
[35] Klasse PJ. How to assess the binding strength of antibodies elicited by vaccination against HIV and other viruses. Expert Rev Vaccines 2016;15(3):295–311.
[36] Karlsson R, Katsamba PS, Nordin H, Pol E, Myszka DG. Analyzing a kinetic titration series using affinity biosensors. Anal Biochem 2006;349(1):136–47.
[37] Karlsson R. Affinity analysis of non-steady-state data obtained under mass transport limited conditions using BIAcore technology. J Mol Recognit 1999;12(5):285–92.
[38] R Core team. R: A language and environment for statistical computing. R Foundation for Statistical Computing; 2018.
[39] Sebaugh JL, McCray PD. Defining the linear portion of a sigmoid-shaped curve: bend points. Pharm Stat 2003;2(3):167–74.